

LoS-Map Construction for Proactive Relay of Opportunity Selection in 6G V2X Systems

Francesco Linsalata, *Student Member, IEEE*, Silvia Mura, *Student Member, IEEE*,
 Marouan Mizmizi, *Member, IEEE*, Maurizio Magarini, *Member, IEEE*, Peng Wang, *Member, IEEE*,
 Majid Nasiri Khormuji, *Senior Member, IEEE*, Alberto Perotti, *Senior Member, IEEE*,
 Umberto Spagnolini, *Senior Member, IEEE*

Abstract—The evolution of connected and automated vehicles (CAVs) technology is boosting the development of innovative solutions for the sixth generation (6G) of Vehicular-to-Everything (V2X) networks. Lower frequency networks provide control of millimeter waves (mmWs) or sub-THz beam-based 6G communications. In CAVs, the mmW/Sub-THz guarantees a huge amount of bandwidth ($>1\text{GHz}$) and a high data rate ($> 10\text{ Gbit/s}$), enhancing the safety of CAVs applications. However, high-frequency is impaired by severe path-loss, and line of sight (LoS) propagation can be easily blocked. Static and dynamic blocking (e.g., by non-connected vehicles) heavily affects V2X links, and thus, in a multi-vehicular case, the knowledge of LoS (or visibility) mapping is mandatory for stable connections and pro-active beam pointing that might involve relays whenever necessary.

In this paper, we design a criterion for dynamic LoS-map estimation, and we propose a novel framework for relay of opportunity selection to enable high-quality and stable V2X links. Relay selection is based on cooperative sensing to cope with LoS blockage conditions. LoS-map is dynamically estimated on top of the static map of the environment by merging the perceptive sensors' data to achieve cooperative awareness of the surrounding scenario. Multiple relay selection architectures are based on centralized and decentralized strategies. 3GPP standard-compliant simulation is the framework methodology adopted herein to reproduce real-world urban vehicular environments and vehicles' mobility patterns.

Index Terms—6G, V2X, CAV, mmW, relay selection

I. INTRODUCTION

CONNECTED and Automated Vehicle (CAV) technology will revolutionize the transportation system by providing a safer, more efficient, and less polluted road environment. CAV's main distinguishing features are the availability of various on-board sensors (e.g., Lidar, Radar, cameras, etc.) for environment perception and the enhancement of the Vehicle-to-Everything (V2X) communication capabilities [1, 2, 3]. Current V2X systems are mainly based on two alternative Radio Access Technologies (RATs): i) Dedicated Short Range Communications (DSRC) sponsored by IEEE [4] and ii) Cellular V2X (C-V2X) promoted by the 3rd Generation Partnership

F. Linsalata, S. Mura, M. Mizmizi, and M. Magarini are with Dipartimento di Elettronica, Informazione e Bioingegneria, Politecnico di Milano, Via Ponzio 34/5, 20133, Milano Italy.

P. Wang, M. N. Nasiri, and A. Perotti are with Huawei Technologies Sweden AB, Skalholtsgatan 9-11, SE-164 94 Kista, Stockholm, Sweden

U. Spagnolini is with Dipartimento di Elettronica, Informazione e Bioingegneria, Politecnico di Milano, Via Ponzio 34/5, 20133, Milano Italy and Huawei Technologies as Huawei Industry Chair.

Project (3GPP) [5]. Both standards operate at sub-6 GHz frequencies, i.e., Frequency Range 1 (FR1), and can only meet the requirements of basic V2X services due to the limited bandwidth [6]. 6G V2X is expected to support a wide range of services, i.e., enhanced-V2X (e-V2X), with increasingly stringent requirements: $> 10\text{ Gbps}$ per link, $< 1\text{ ms}$ latency, and $< 1 \cdot 10^{-9}$ reliability [7]. To address these new demands, the 3GPP has launched 5G New Radio (NR) V2X Rel. 16 [8] and further enhancements from Rel. 17 [9] are under discussion. The most significant innovation in Rel. 17 is the possibility of exploiting mmW frequencies (24.25 GHz-52.6 GHz), i.e., Frequency Range 2 (FR2), to support bandwidth-demanding applications. Furthermore, sub-THz (90-300 GHz) are being studied for 6G V2X communications [10, 11].

Propagation at such high frequencies is subject to severe attenuation and mostly requires an LoS condition. Indeed, blockage is the most relevant limitation for the range covered and for communication reliability [12, 13]. Massive Multiple-Input Multiple-Output (MIMO) systems are promising solutions for high-frequency communication, enabling a beam-type communication capable of achieving high antenna gain. Beams need to be collimated. Beam alignment and tracking are key issues, mostly in a dynamic environment as in vehicular scenarios, where frequent beam misalignments and blockages occur, with a detrimental effect on the system's performance [14].

Beam blockage can be mitigated by relaying mechanisms [13, 15, 16], for example, from nearby CAVs, Road Side Units (RSU), or Intelligent Reflecting Surfaces (IRS) [17]. Relay selection strategies can be grouped into two macro-categories: *i*) centralized [18, 19]: a network entity, such as Next Generation Base Station (gNB) or an elected vehicle, acts as a *central body* (CB) that collects network state and defines the optimal relay selection; *ii*) distributed [20, 21, 16]: each vehicle computes the ego optimal relay and attempts to directly interact with it.

This paper proposes a proactive relay of opportunity selection that has been adopted for both centralized and distributed schemes.

Related Works

Many works in literature approach relay selection by abstracting the physical layer. The authors in [22] propose a distributed vehicular relay selection strategy assuming a

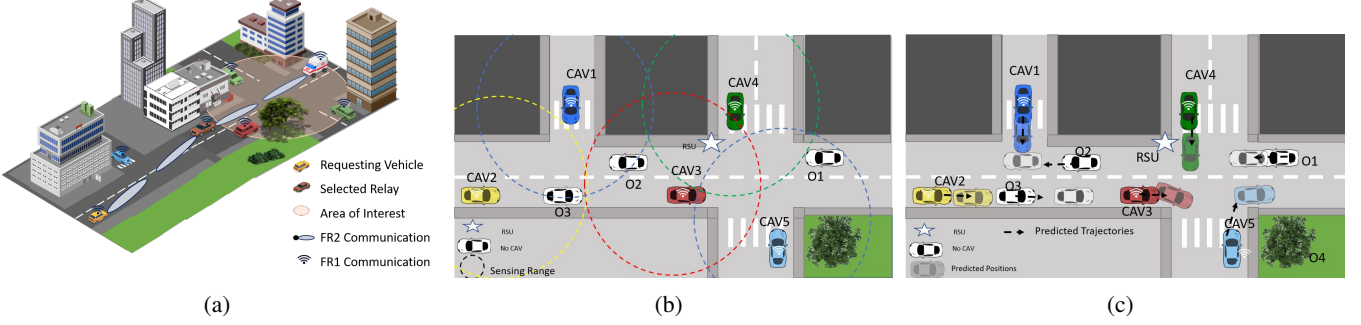


Figure 1: V2X extended sensing between RV (e.g. yellow and blue car) and VoI (e.g. red and green cars). In (a) the scenario at the collection phase instant, in (b) the Cooperative Awareness Signalling to enable cooperative sensing, and in (c) the predicted trajectories based on CA signalling and maneuvers- and physical-based models.

Nakagami fading channel. A moving-zone-based architecture is proposed in [19], where the CB is elected from the set of vehicles. The CB establishes communication with the closest relay to the destination by using the Dijkstra algorithm. In [23] the channel state information at the communication antenna is predicted based on a predictor antenna that is a second antenna mounted on the CAV's front bumper. The presence of a predictor antenna can boost communication performance. However, the prediction time horizon depends on the speed of the CAV and the distance between predictor and communication antennas, which is limited by the size of the CAV. In [24], the authors assume that each vehicle equipped with a GPS receiver can download the digital maps from the cloud. Their combination can be used to choose from the neighbors a relay node that is strategically located in the perfect-reception zone. However, they assume the absence of old branded non-connected cars that can interrupt the link.

In order to overcome the LoS blockage problem at mmW, in [25] the authors propose using neighbouring vehicles as relays to forward the blocked traffic flows. Specifically, a traffic-aware relay vehicle selection is investigated, by combining the results of an analytic hierarchy process and coalitional game. A heuristic relay selection scheme is devised to select the relay vehicle with the best rationality degree. However, the analysis considers a limited road section and lacks realistic system model and mobility patterns.

A common drawback of the works concerning the relay-assisted mmW V2X communications is the widespread use of stochastic models of the channel. This is very limiting in modelling the complex real-world scenario. For example, stochastic channels do not account for the impact on the system's performance of *dynamic blockers*, such as moving vehicles and pedestrians. In [26], the authors use a Network Simulator 3 (NS-3) [27] mmW module and 5G Lena [28] for simulating V2I communication, focusing only on cellular-like and infrastructure-based deployments. The work in [29] proposes MilliCar, an open-source simulator for a Vehicle-to-Vehicle (V2V) scenario with a mmW channel, full TCP/IP protocol stack, and vehicles' mobility. Again, the stochastic channel description fails in capturing the dynamic system's complexity. Coverage, mobility, and blockage are studied in [30] by exploiting a 3D ray-tracer to accurately reproduce

the mmW channel propagation [31]. The simulation architecture achieves high performance in replicating the channel propagation model but its high complexity fails to capture the insight of the dynamics for relay scheduling design.

Contributions

This paper is contextualized in the future 6G-enabled CAV applications/services where CAVs share sensor data to improve the perception of the surrounding environment. CAVs are equipped with two communication interfaces: mmW/Sub-THz beam-type communication for high data rate and a sub-6 GHz for signalling and control [32] as depicted in Fig. 1a. This paper's main contributions can be summarized as follows:

- The proposed approach leverages on cooperative sensing to predict the LoS-map of the V2X network and to design a countermeasure to beam blockage. The static objects (e.g., buildings and trees) in the LoS-map can be retrieved either from the 3D maps downloaded from edge server or by the CAVs' on-board sensors. The trajectories of dynamic objects, such as non-cooperative vehicles and pedestrians, are derived by adapting the motion prediction algorithms in [33, 34, 35]. The vehicles' mobility and the uncertainty on the objects' position lead to dynamic LoS conditions. This depends on the CAV density and impacts on the corresponding V2X connectivity.

- The distribution of the LoS-map has been derived analytically for one V2X scenario. Instantaneous network connectivity for a dynamic vehicular mesh has been evaluated in the conditions of no relaying (lower bound) and optimal relaying (upper bound). This enables comparison of different relaying techniques, both centralized and distributed, under various link conditions and resource constraints.

- A unified simulation methodology of mmW V2X networks is proposed. The modelling of vehicle traffic over real road networks is obtained by using a combination of Open-StreetMap (OSM) [36] and Simulation of Urban MObility (SUMO) [37] software. Furthermore, the output of SUMO is processed by the Geometry-based, Efficient Propagation Model for Vehicle-to-Vehicle (GEMV²) [38] software, in which the radio propagation has been adapted according to the latest 3GPP guidelines in [39]. All numerical results are based on this integrated simulation environment.

Organization

The rest of this paper is organized as follows. Section II introduces the methodology, while Sec. III deals with the network connectivity analysis. Section IV gives an overview of centralized relay selection schemes, while Sec. V focuses on the distributed relay selection schemes. Section VI describes the implemented simulation set-up with scenario definition and the CAVs' data sharing studied cases. Numerical results and complexity analysis are investigated in Sec. VII. Lastly, Sec. VIII summarizes and concludes the work.

Notation

Bold upper and lower-case letters describe matrices and column vectors, respectively. $[\mathbf{A}]_{(i,j)}$ denotes the (i,j) entry of matrix \mathbf{A} . Transposition and conjugate transposition are denoted with the operator $(\cdot)^T$ and $(\cdot)^H$, respectively. The determinant of matrix \mathbf{A} is $\det(\mathbf{A})$. $\text{tr}(\mathbf{A})$ extracts the trace of matrix \mathbf{A} . $|\cdot|$ is the cardinality of a matrix or a set, i.e. its number of elements. With $\mathbf{a} \sim \mathcal{CN}(\boldsymbol{\mu}, \mathbf{C})$ we denote a multivariate complex Gaussian random variable \mathbf{a} with mean $\boldsymbol{\mu}$ and covariance \mathbf{C} . \mathbf{I}_N stands for the identity matrix of dimensions N . The functions $f_X(x)$ and $F_X(x)$ define the probability density function (pdf) and cumulative density function (cdf) of a random variable X , respectively. The notation $m^{(i,j)}$ is used to indicate a metric m of the link between the (i,j) th communication couple, while p^i associates the parameter p to the i th CAV, RSU, and/or object.

II. METHODOLOGY

This section introduces the proposed method for relay of opportunity selection, based on prediction of the LoS-map. First, leveraging on the static information and cooperative perception of CAVs, the upcoming network state is estimated. Then, the predicted links availability is used to determine the V2X network connectivity, achieved using relaying schemes.

A. Study Case

CAVs are assumed to be equipped with two communication interfaces: *i*) a low data-rate and omnidirectional communication interface for Cooperative Awareness (CA) messages, dissemination and signalling (e.g., 5G NR in FR1); *ii*) a high data-rate and beam-based communication interface for raw sensor data sharing (e.g., 5G NR in FR2 or 6G Sub-THz). Moreover, each CAV is assumed to share its planned trajectory with nearby CAVs.

Figure 1 depicts the considered scenario with sketched beams. We consider V2X extended sensing as the 3GPP use case [39]. The CAVs exchange raw or nearly raw sensor data to achieve an augmented perception. More specifically, a Requesting Vehicle (RV) can establish direct access to the sensor of a Vehicle of Interest (VoI) after creating an Over-the-Air data bus, or virtual data bus [40] for sensor data exchange. A CAV that is approaching a certain critical area, e.g., road intersection or roundabout, requires augmented perception of the objects/obstacles present in the scene and their state to perform a safe manoeuvre. By referring to Fig. 1a, we denote

the critical area as the Area of Interest (AoI), the collaborating CAVs as VoI (e.g., green and red cars in Fig. 1a), and the approaching CAVs as RVs (e.g., blue and yellow cars in Fig. 1a). The VoIs inside the intersection (or roundabout) possess an advantageous point of view of that road segment's traffic flow. The incoming vehicles (i.e., RVs), on the other hand, are entering a critical road area, and need to gather as much perceptive information as possible.

B. Cooperative LoS-map Sensing

The on-board sensing capability of each CAV is exploited to perceive the surrounding static and dynamic blockers at a specific time instant t_0 . This information is then exchanged using the FR1 communication interface to obtain the cooperative sensing of the objects. The signalling to accomplish cooperative sensing has been standardized by the Intelligent Transportation System (ITS) society for CAVs, mainly for safety-related use cases. Vehicles can exploit three types of Cooperative Awareness (CA) signaling, i.e., Cooperative Awareness Message (CAM), Decentralized Environmental Notification Message (DENM), and Cooperative Perception Messages (CPM). CAMs enable mutual awareness between CAVs and detected obstacles, DENMs are event-based messages containing information related to a road hazard or abnormal traffic conditions, and CPMs contain self-information, such as the available on-board sensors, sensors range, sensors field of view, position, speed, heading, and size of the detected objects [41].

In particular, for each detected object k at time instant t_0 , the i th CAV estimates its position $(\tilde{x}_i^k(t_0), \tilde{y}_i^k(t_0))$ and speed $\tilde{v}_i^k(t_0)$ along x and y directions of the Cartesian plane. These parameters define the state of the k th object, which is represented as the column vector

$$\tilde{\mathbf{s}}_i^k(t_0) = [\tilde{x}_i^k(t_0), \tilde{y}_i^k(t_0), \tilde{v}_{i,x}^k(t_0), \tilde{v}_{i,y}^k(t_0)]^T \quad (1)$$

that due to the measurement uncertainty can be approximated as $\tilde{\mathbf{s}}_i^k(t_0) \sim \mathcal{N}(\mathbf{s}_{true}^k(t_0), \tilde{\Sigma}_i^k(t_0))$ where $\mathbf{s}_{true}^k(t_0)$ is the true state of the k th object [42].

The list of K objects $\mathcal{L}_i = \{\tilde{\mathbf{s}}_i^1(t_0), \dots, \tilde{\mathbf{s}}_i^K(t_0)\}$ detected by the i th CAV and their spatial footprint (see Remark 1) are signalled by leveraging on CA messages through the FR1 interface.

An estimate of the state associated with the k th object is obtained by each CAV (for a distributed architecture) after reaching cooperative consensus or by the CB (in case of a centralized architecture). Assuming the presence of N_c CAVs, the initial state of the k th object is approximated as

$$\tilde{\mathbf{s}}^k(t_0) \sim \mathcal{N}(\mathbf{s}_{true}^k(t_0), \tilde{\Sigma}^k(t_0)), \quad (2)$$

where the covariance matrix is

$$\tilde{\Sigma}^k(t_0) = \left(\sum_{i=1}^{N_c} \tilde{\Sigma}_i^k(t_0) \right)^{-1}. \quad (3)$$

We state that in the proposed framework, the CA signalling at FR1 is exploited to support the communication at mmW

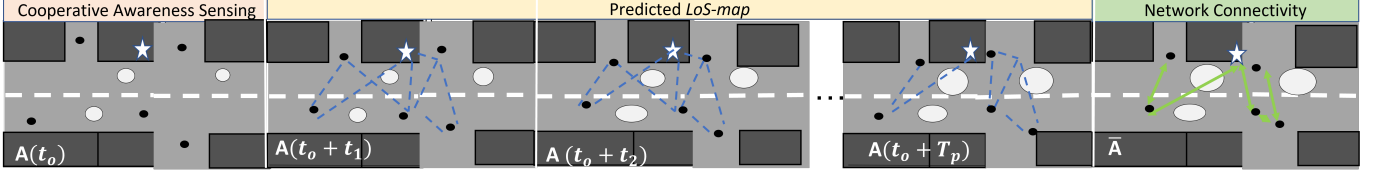


Figure 2: V2X network evolution while moving: after sensing, each CAV knows the others' state (black dots); the metrics based on predicted trajectories (black for CAV and white dots for old branded cars) are used to build an adjacency matrix $\mathbf{A}(t)$ for each time instant t , the entries of $\mathbf{A}(t)$ represent the service probability of the communication links involving CAVs and RSU, and it depends on the SNR $\gamma(t)$.

frequency (e.g., in Fig. 1b). In fact, by combining the CA-based information and the blockers states, each CAV can evaluate its static LoS-map at t_0 and predict the dynamic LoS-map in $[t_0, t_0 + T_p]$, estimating the LoS condition between each tuple (i, j) of CAVs in the network over the prediction time window T_p . The LoS condition classification from 3GPP standards depends on the obstacle type; therefore, the link between the two CAVs can be classified as NLoSb/NLoSf in the case of building or foliage blockage, NLoSv in case of vehicle blockage, and as LoS if no blockage is affecting the link.

Remark 1. Each CAV that measures the state of a k th object needs to estimate its spatial footprint. For an nCAV, its localization of the point $(\tilde{x}_i^k(t_0), \tilde{y}_i^k(t_0))$ has an intrinsic uncertainty within the vehicle's shape. The uncertainty results in a convolution between the normal distribution of an estimate point [42] and the vehicle's shape. The result can be approximated to a normal bivariate for high uncertainty. Thus, the footprint area of the vehicle can be modelled by an isotropic disc of radius $\sigma_i^k(t_0)$, whose value is taken into account in the initialization of the covariance matrix $\tilde{\Sigma}_i^k(t_0) = \sigma_i^k(t_0)^2 \mathbf{I}$. These considerations allow us to adopt Gaussian models.

C. Prediction of the LoS-map

The cooperative sensing information collected makes it possible to predict the state of non-connected vehicles (nCAVs) in the time window T_p . Many prediction strategies are discussed in literature. The proposed method revises and reshapes the work in [34, 33, 43], where the predicted state at time instant \bar{t} is

$$\tilde{\mathbf{s}}^k(\bar{t}) = \mathbf{T}(\bar{t})\tilde{\mathbf{s}}^k(t_0) + \mathbf{w}^k(\bar{t}), \quad (4)$$

where

$$\mathbf{T}(\bar{t}) = \begin{bmatrix} \mathbf{I}_2 & \bar{t} \mathbf{I}_2 \\ \mathbf{0}_{2 \times 2} & \mathbf{I}_2 \end{bmatrix} \quad (5)$$

is the transition matrix of the dynamic model and $\mathbf{w}^k(\bar{t}) \sim \mathcal{N}(\mathbf{0}, \mathbf{Q}^k(\bar{t}))$ is the driving random process in case of a constant velocity motion model. The random process is assumed Gaussian, with \mathbf{Q}^k detailed in [44].

The proposed framework, depicted in Fig. 2, exploits the predicted states to evaluate the dynamic evolution of LoS conditions among CAVs over the time window T_p .

D. Network Metrics Evaluation

The QoS of the link can be characterized by its SNR $\gamma^{(i,j)}(t)$. For simplicity of notation, the indexes (i, j) that identify a certain link will be omitted since the discussion can be generalized for any tuple of CAVs. The time evolution of γ depends on configurable parameters, such as transmission power and antenna gain, and non-configurable ones, such as the distance between transmitting and receiving CAVs and blocking obstacles. Static obstacles are inferred from the digital map and CA signalling, while the state of dynamic nCAVs is predicted in (4). The predicted motions make the LoS-map dynamically evolving over time (see Fig. 2).

We assume that CAVs are equipped with $N_a = N_v \times N_c$ cylindrical antenna arrays on their rooftop, where N_v is the number of uniform circular arrays, characterized by N_c uniformly spaced antenna elements each as defined in [47] (any other array configuration needs a straightforward adaptation). The SNR at time \bar{t} in decibel scale is

$$\begin{aligned} \gamma(\bar{t}) &= P_{Tx} + 2G_b - PL(\bar{t}) - P_n = \\ &= \gamma_0(\bar{t}) - PL(\bar{t}) \quad [\text{dB}] \end{aligned} \quad (6)$$

where P_{Tx} is the transmitted power, G_b is the antenna gain, P_n is the noise power, and path-loss $PL(\bar{t}) \sim \mathcal{N}(A_{LoS}(d(\bar{t})), \sigma_{sh}^2)$ contains log-normal shadowing with variance σ_{sh}^2 and $A_{LoS}(d(\bar{t}))$ in Table I. The randomness of the SNR is analyzed next.

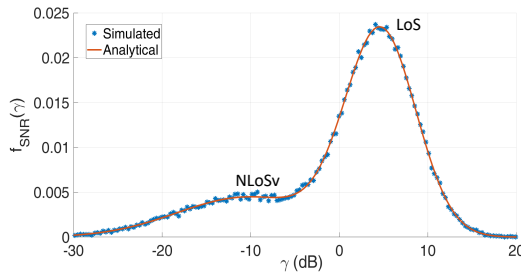
Remark 2. In the case of multiple blockages, the order of relevance in the $PL(\bar{t})$ computation depends on the blocker with the highest attenuation [39, 48], in order (from Table I): NLoSb, NLoSf, and lastly NLoSv. For example, if the LoS is blocked by a building and a vehicle, the used path-loss model is NLoSb.

E. Link SNR statistics

In our framework, current and future positions of all CAVs are considered known with negligible error. This assumption is based on the localization and tracking systems of self-driving CAVs that combine multiple sensors to reach sub-metre position accuracy, including the individual footprints with exact shapes [49, 50]. Furthermore, self-driving cars know their future trajectory as it is typically self planned [34, 33, 43]. The SNR γ distribution, based on the LoS condition, is affected by the uncertainty of the nCAVs positions and shadowing.

Table I: Direct component characterization of the path-loss models from 3GPP [39, 45, 46]

Condition	Mean value ($A_{PL}(d)$) [dB]	Symbol	Description
LoS	$32.4 + 20 \log_{10}(d) + 20 \log_{10}(f)$	$A_{LoS}(d)$	clear link visibility
NLoSb	$36.85 + 30 \log_{10}(d) + 18.9 \log_{10}(f)$	$A_{NLoSb}(d)$	buildings blockage
NLoSf	$A_{LoS}(d) + A_f$	$A_{NLoSf}(d)$	foliage obstructions
NLoSv	$A_{LoS}(d) + A_v$	$A_{NLoSv}(d)$	vehicular blockage

Figure 3: Analytical and numerical SNR γ pdf

In the following section, we evaluate the pdf of the SNR in closed form. Two illustrative cases are considered below for the dynamic LoS-map:

- **absence of nCAVs:** the SNR distribution (in decibel scale) $f_{SNR}(\gamma)$ for the LoS and NLoSb/f cases is

$$f_{SNR}(\gamma) = \mathcal{N}(\gamma_0 - A_{PL}(d), \sigma_{sh}^2), \quad (7)$$

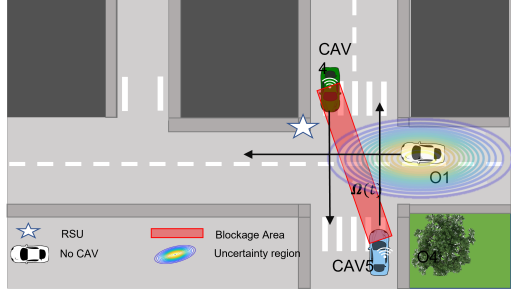
with the variance σ_{sh}^2 related to the shadowing. In case of LoS and NLoSb the term $A_{PL}(d)$ is reported in Tab. I, while for NLoSf, the path-loss PL in (6) contains an additive random term $X_{extra} \sim \mathcal{N}(A_f, \sigma_f^2)$. The extra attenuation due to the foliage A_f is computed using the concept of mean excess loss derived in [46] and the overall path-loss distribution results in $PL \sim \mathcal{N}(A_{LoS}(d) + A_f, \sigma_f^2 + \sigma_{sh}^2)$.

• **presence of nCAVs:** the SNR distribution $f_{SNR}(\gamma)$ depends on the shadowing component and the probability of blockage due to nCAVs. The extra attenuation for vehicular blockage A_v depends on the number of blocking vehicles [39]. The path-loss distribution is evaluated similarly to NLoSf case. The SNR pdf $f_{SNR}(\gamma)$ can be computed as

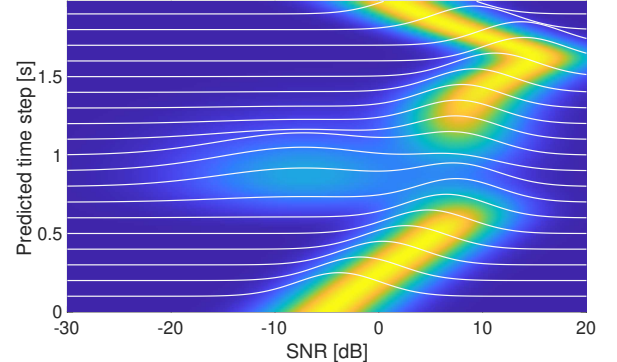
$$f_{SNR}(\gamma) = P_{LoS} f_{LoS}(\gamma) + \sum_{k_b=1}^{N_b} P_{NLoSv}^{(k_b)} f_{NLoSv}^{(k_b)}(\gamma), \quad (8)$$

where the term P_{LoS} is the probability of LoS condition, $f_{LoS}(\gamma)$ is the related SNR pdf, $P_{NLoSv}^{(k_b)}$ is the probability of having k_b nCAVs blockers out of N_b nCAVs, and $f_{NLoSv}^{(k_b)}(\gamma)$ is the related SNR pdf. The pdf in (8) is a mixture of Gaussians. P_{LoS} and $P_{NLoSv}^{(k_b)}$ are complementary: $P_{LoS} + \sum_{k_b=1}^{N_b} P_{NLoSv}^{(k_b)} = 1$. Their analytical derivation, together with the the LoS and NLoSv SNR pdfs, are derived in Appendix A. Figure 3 shows the analytical and simulated behaviour of the SNR pdf in (8) for single blockage, i.e., $k_b = N_b = 1$.

Figure 4a illustrates a realistic use-case where the link between two CAVs can be obstructed by a nCAV (O1). Its SNR distribution varies according to the vehicles' relative



(a) Scenario of uncertainty between LoS and NLoSv



(b) SNR pdf versus prediction time

Figure 4: CAVs link pair SNR pdf evolution according to the predicted positions in case of uncertainty between LoS and NLoSv.

motion directions (black arrows). The pdf of the SNR for every prediction time instant \bar{t} is reported in Fig. 4b. It can be seen that, as soon as the nCAV uncertainty region is expected to intersect the blockage area (red polygon), the SNR drops as shown by the slices at $t \in (0.6, 1.2)$ s, and after the nCAV departure the SNR rises again.

III. PREDICTED NETWORK CONNECTIVITY

Once the SNR distribution of each link associated with the LoS-map has been predicted, the adjacency matrix of CAVs' network is used to compute the connectivity. The entries of the adjacency matrix are defined by the probability that SNR pdf is higher than a threshold γ_{th} , which is the minimum QoS according to the specific V2X service. The adjacency matrix is then used as input of the relay selection strategies.

A. Network Adjacency matrix

The predicted pdfs of SNR $\gamma^{(i,j)}(t)$ are used to derive the adjacency matrix $\mathbf{A}(t) \in \mathbb{R}^{N_c \times N_c}$ of the CAVs' network in Fig 2. The entries of the matrix $\mathbf{A}(t)$ are the service

probabilities that evolve with the LoS-map (or equivalently, with the motion of the vehicles):

$$[\mathbf{A}]_{(i,j)}(t) = \Pr\{\gamma^{(i,j)}(t) > \gamma_{\text{th}}\} = F_{\text{SNR}^{i,j}}(\gamma_{\text{th}}), \quad (9)$$

with $i, j = 1, \dots, N_c$ and $i \neq j$, and the cdf of the SNR $F_{\text{SNR}}(\gamma_{\text{th}})$ easily follows from (8), as derived in Appendix A. The network performance for link-selection, as described in Sec. IV, is based on the service probabilities in (9) over the communication interval $(t_0, t_0 + T_p]$, which is in turn discretized with sampling interval T_s . Averaging the service probabilities (9) over $N_s = T_p/T_s$ samples of the prediction window, we obtain the *link availability* that is

$$[\bar{\mathbf{A}}]_{(i,j)} = \frac{1}{N_s} \sum_{n=0}^{N_s-1} [\mathbf{A}]_{(i,j)}(t_0 + nT_s). \quad (10)$$

The matrix of the link availabilities $\bar{\mathbf{A}}$ is symmetrical, and it is the key metric for the link selection optimization problems (dealt with later in Secs. IV and V).

B. Connectivity Analysis

The network connectivity is a metric to evaluate any need for relay nodes. Let the metric $\alpha(\bar{\mathbf{A}})$ be the measure of the connectivity of the network, $\alpha(\bar{\mathbf{A}})$ is related to the density of nCAVs and determines a-priori the reliability of the vehicles configuration and mesh of CAVs connectivity. The connectivity can be evaluated by calculating the Laplacian matrix [51]

$$\Delta \stackrel{\text{def}}{=} \mathbf{D} - \bar{\mathbf{A}}, \quad (11)$$

where the elements of \mathbf{D} are the vertex outdegrees

$$[\mathbf{D}]_{(i,i)} = \sum_{j \neq i} [\bar{\mathbf{A}}]_{(i,j)}. \quad (12)$$

The second smallest eigenvalue λ_2 of Δ defines the network connectivity $\alpha(\bar{\mathbf{A}}) = \lambda_2$, which is $\alpha(\bar{\mathbf{A}}) > 0$ in case of connected network.

The second order connectivity determines the network's robustness by also taking into account a 2-hops link to connect two nodes. It is obtained by substituting $\bar{\mathbf{A}}$ with $\bar{\mathbf{A}}_2$ that is defined as

$$\bar{\mathbf{A}}_2 = \bar{\mathbf{A}}^2 - \bar{\mathbf{A}}. \quad (13)$$

This can be interpreted as a performance upper-bound for the relay schemes' connectivity capability.

We study the first order connectivity in the highway scenario in Fig. 5a since it is characterized by simpler topology and mobility trajectories with respect to the urban environment. The simulation is performed by varying the traffic density and CAV density ρ_c with γ_{th} equal to 10dB. The number of considered vehicles and the percentage of CAVs and nCAVs are control variables such that the CAV density is

$$\rho_c = \frac{N_c}{N_b + N_c}. \quad (14)$$

In this example, a V2X network, which admits only direct links, exhibits poor robustness when the traffic density grows and 50% of the total vehicles are nCAVs (Fig. 5b). However, if two-hops links are admitted, the connectivity approaches

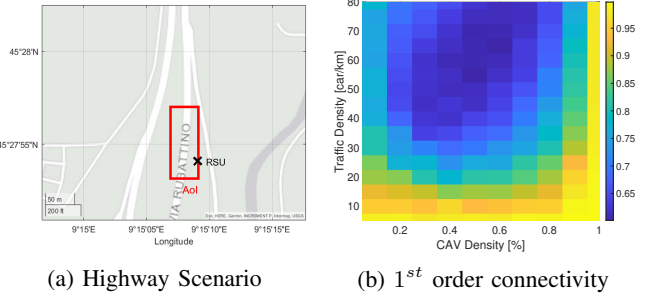


Figure 5: First order network connectivity versus CAV density ρ_c in percentage for different traffic density condition.

the maximum, resulting in more robust V2X network. These results outline the need for opportunistic relay selection strategies that involve not only the network infrastructure (RSU) but also CAVs. This will be more urgent in the next decade when the market penetration of CAVs is expected to be low. These considerations are also eligible for urban intersection and roundabout scenarios, where opportunistic relaying schemes are more useful because of the presence of both dynamic and static blockers. Possible relay of opportunity strategies are highlighted in the next sections.

IV. PREDICTIVE CENTRALIZED APPROACH

Centralized link selection strategies require overall knowledge of the network state to address the following issues: *which CAVs request a link? Which CAVs are available to act as relay nodes? How CAVs are connected in the network?* Typically, a CB, such as an elected CAV, the BS, or the RSU, through periodical FR1 communications, is responsible for (i) collecting the network information, link requests, and relaying capabilities, (ii) applying the selection algorithm and (iii) communicating the decision to the involved communication parties. In this section, we first introduce the communications signalling required for information gathering and distribution of decisions. Later, we discuss the proposed algorithms for link selection.

A. Centralized protocol

Figure 6 depicts an example time flow for the centralized protocol, i.e., the messages and procedures supporting link selection. In particular:

1) **Cooperative Sensing:** the i th CAV, after the sensing operation, obtains a list of sensed objects \mathcal{L}_i that is sent to the CB together with the CAV relaying capability R_C^i , which represents the maximum number of links it can support as a relay.

2) **Dynamic objects prediction:** the CB, after combining the received lists \mathcal{L}_i for each k th object (e.g., pedestrian, CAV, and nCAV), predicts the dynamic evolution of the sensed nearby objects over a predefined time window T_p , as discussed Sec. II-C.

3) **Network metric evaluation:** CB evaluates, for each predicted time step \bar{t} , the $\gamma^{(i,j)}(\bar{t})$ between each tuple (i, j) of CAVs in the network. The $\gamma^{(i,j)}(\bar{t})$ is computed using (6).

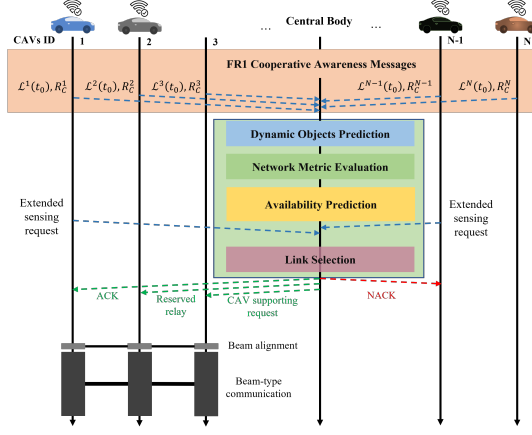


Figure 6: Centralized approach time flow example. CAVs ID1 and IDN-1 are RVs, ID3 is a VoI, and ID2 is a relay. Dashed lines are FRI communication links, while continuous lines represent beam-type communication, e.g. FR2.

4) **Prediction of dynamic adjacency matrix** is derived by the CB based on the previously estimated SNRs. The entries of the adjacency matrix are computed based on (9).

5) **Link selection:** CAVs (i.e., RVs) that plan to cross an AoI could send a request for extended sensing to the CB, as depicted in Fig. 6. The CB collects the received requests and provides the optimal link based on the predicted link availability in (10) and on the link selection algorithm. If this link exists, the CB sends an acknowledgment (ACK) to the RV (otherwise, it sends a NACK), a request to the CAV supporting extended sensing, and a relay reservation request. Finally, the CB sends the necessary information to establish an FR2 communication link to the involved parties, as in Fig. 6.

The centralized protocol is executed periodically so that the information obtained through cooperative sensing is updated, and, consequently, the network metrics and the predicted link availability.

B. Centralized link selection

The link selection algorithm plays a key role in this framework. For the centralized approaches, two algorithms are detailed below:

• **Congestion games:** are a particular class of *potential games* [52] used to describe a situation where a set of N players need to perform a certain *task* using some resources in a set R . In the considered study case, the requesting vehicles (RVs) are the *players*, the *task* is the communication toward vehicles of interest (VoIs), while the relays play the role of *resources*. By calling $\mathbf{m} = (m_1, \dots, m_N)$ a possible strategy profile, whose elements belong to the corresponding strategy space $\mathcal{M}^i = (r_1^i, r_2^i, \dots, r_m^i)$ of player i , each relay $r \in R$ has a cost c_r determined by the number of players n_r using resource r . The cost c_r depends on the strategy profile \mathbf{m} as

$$c_r(n_r) = \begin{cases} 2n_r, & \text{if } n_r \leq R_C^r, \\ \infty, & \text{otherwise,} \end{cases} \quad (15)$$

where R_C^r is the relaying capability of the r th relay, representing the maximum number of supported links. The optimal strategy is obtained by minimizing w.r.t \mathbf{m} the total cost, which is the potential function of the game [52]

$$P(\mathbf{m}) = \sum_{i=1}^N u_i(\mathbf{m}), \quad (16)$$

where the payoff function of the i th player $u_i(\mathbf{m})$ is the sum of the costs

$$u_i(\mathbf{m}) = \sum_{r \in m_i} c_r. \quad (17)$$

The game's complexity is computed by assuming that the strategy space cardinality of each RV equals to $\frac{M}{N}$, with $M = \sum_i^N |\mathcal{M}^i|$. In [53] the authors show that finding the Nash equilibrium in the congestion game problem is NP-hard, and the computational complexity is $\mathcal{O}(M^N N^{-N})$.

• **Hungarian games:** belong to the family of linear assignment problems

[54]. The input is a non-negative $N \times M$ matrix \mathbf{C} , where the i th row corresponds to the *task*, i.e., the communication link between a RV and a VoI, while each j th column represents a *resource*, which is a relay for the i th communication link. The entry $[\mathbf{C}]_{(i,j)}$ is the cost of assigning relay j to the communication link i , and it is a function of the link availability in (10) as

$$[\mathbf{C}]_{(i,j)} = \frac{1}{[\bar{\mathbf{A}}]_{(i,j)}}, \quad (18)$$

The optimization algorithm aims to minimize the total assignment cost. This can be obtained by finding the rows and columns permutations that minimize the trace of \mathbf{C}

$$\min_{\mathbf{L}, \mathbf{R}} \text{tr}(\mathbf{L} \mathbf{C} \mathbf{R}), \quad (19)$$

where \mathbf{L} and \mathbf{R} are the possible permutation matrices. This approach solves a linear assignment problem, which limits a relay to be assigned to only one communication link pair. Hungarian game has a polynomial run-time complexity. Generally, the algorithm performs the optimal assignment between rows and columns achieving social optimality with a computational complexity that is $\mathcal{O}([\min(N, M) |\mathbf{C}|])$ [55]. For a dense urban scenario we usually have $N \leq M$. Therefore, the computational complexity is $\mathcal{O}(N^2 M)$.

V. PREDICTIVE DISTRIBUTED APPROACH

Distributed link selection approaches do not rely on a CB. CAVs individually compute the optimal link locally and compete for the available relays.

A. Distributed protocol

The time flow of the proposed distributed architecture (Fig. 7) is similar to the centralized one. The main differences are related to cooperative sensing and link selection that are executed locally by the RVs only. In particular:

1) **Cooperative sensing:** differently from the centralized method, each CAV shares with neighbouring CAVs the list of detected objects \mathcal{L}_i and its relaying capability R_C^i .

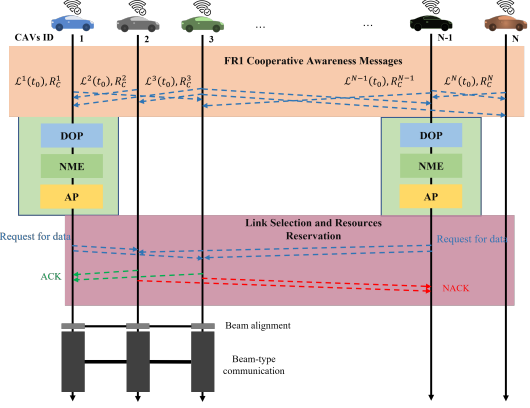


Figure 7: Distributed approach time flow example. CAVs ID1 and IDN-1 are RVs, ID3 is a VoI, and ID2 is a relay. Dashed lines are FR1 communication links, while continuous lines represents beam-type communication, e.g., FR2.

2) **Link selection and resources reservation:** each RV executes the link selection algorithm based on the predicted link availabilities in (10). The RVs send resources reservations requests to the selected relays, as depicted in Fig. 7. The relays, based on their available relaying capabilities, reply to the RVs with positive or negative feedbacks.

As for the centralized case, the distributed protocol is executed periodically to update the cooperative sensing information and the predicted link availability.

B. Distributed link selection

Two strategies are considered for the distributed link selection architecture:

- **First Come First Served (FCFS):** is based on the *first input first output* scheduling strategy. Each RV sorts the links according to their availabilities. The RV sends the request for resource reservation to the relay associated to the link with maximum availability. If the relay's capability is sufficient, it sends a ACK, otherwise a NACK. The relays are assigned sequentially.

The computational complexity is $\mathcal{O}(M)$.

- **Auction-based game:** is a distributed multi-buyer multi-seller game [56] in which N *buyers*, i.e. the RVs, concur for the available *sellers*, i.e. the relays. Each RV makes a bid for the relay that guarantees the best trade-off between service price and availability at each k th auction iteration, with $1 \leq k \leq T_k$. The service price c_r of the relay capability resources increases with the number of bids made at each iteration as

$$c_r(k+1) = c_r(k) \exp \left(\frac{\zeta_r(k)}{\eta_r(k)} \right), \quad (20)$$

where $\zeta_r(k)$ identifies the number of requested resources, while $\eta_r(k) \in [0, R_C^r]$ identifies the relay capability at the k th iteration. The updated service price in (20) is sent as feedback to the buyers. The selection is performed by solving

$$\max_{r \in R} \sum_{i=1}^N \left([\bar{\mathbf{A}}]_{(i,j)} - c_r(k+1) \right). \quad (21)$$

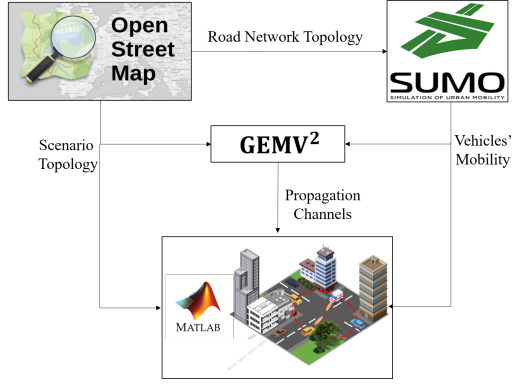


Figure 8: Simulation Methodologies

Table II: Simulation parameters

Parameter	Value	Description
P_{Tx}	10 dBm	Maximum transmitted Power
P_n	-85.5 dBm	Noise power
f_c^1	5.2 GHz	FR1 carrier frequency
f_c^2	28 GHz	FR2 carrier frequency
N_a	4×16	Number of antenna elements
T_p	1 s	Predicted time window
$R_{cav,rsu}^{cav,rsu}$	2	Maximum number of relay requests granted by a CAV and RSU
L	2	Maximum number of hops

Each RV compares the utility and the cost of its possible $\frac{M}{N}$ strategies at each auction iteration [57]. Therefore, the total computational complexity in T_k is $\mathcal{O}(T_k M)$.

VI. SIMULATIONS FRAMEWORK

The mmW V2X communication is characterized by highly dynamic and sparse propagation channels [58, 59], subject to blockage by nCAVs, buildings, and trees. To better capture the system's complexity, the proposed framework combines several tools to simulate a realistic scenario, as depicted in Fig. 8. In particular, the simulation environments, i.e., road network topology, buildings, and vegetation, are obtained from OSM [36]. Realistic vehicular mobility is simulated by SUMO [37], and the GEMV² [38] software generates the wireless channel in Matlab.

This section describes how the software tools are combined and set for numerical validation. Table II reports the main parameters used for the communications by following the 3GPP recommendations in [60].

A. Simulated Scenarios

A blind intersection (Fig. 9a) and a roundabout scenario (Fig. 9b) are deemed to evaluate the performances of the proposed relay selection schemes. The selected areas are located around the city of Milan, Italy. For each scenario, the AoI represents the critical area in the road environment. The CAVs, whose sensors' field of view is within the AoI are the VoIs. The range of the AoI (red circle) in the intersection and roundabout is 30 m and 90 m, respectively, and depends on the road patterns. The RSUs are deployed in strategic positions, e.g., in the centre of the roundabout (see Fig. 9), to assist the communication.



Figure 9: Simulated urban blind intersection (a) and roundabout (b).

Table III: SUMO mobility parameters

Parameter	Urban	Highway
Time step T_s	10 ms	10 ms
Time duration	300 s	300 s
Number of vehicles	277	145
Vehicles flow	2 veh/s	1.5 veh/s
Maximum speed	50 km/h	130 km/h

B. Vehicles Topology and Mobility

Simulation of vehicles' mobility is performed by SUMO software that allows for realistic traffic data generation. The *road network*, used as input to SUMO, is generated from the selected OSM scenario. SUMO parameters for the selected scenarios are reported in Tabs. III- IV. The output is processed in MATLAB together with the OSM scenario.

C. V2X Communications Channel

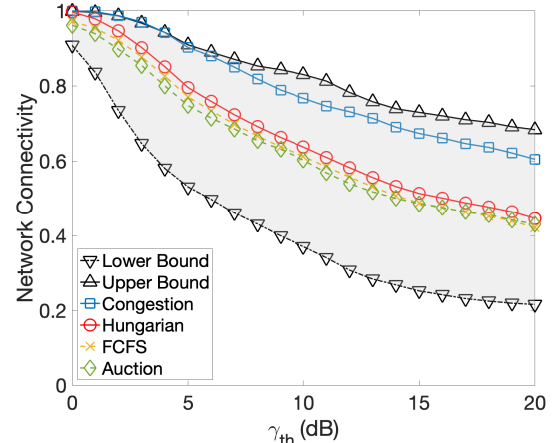
GEMV² [38] is an open-source solution for V2X channel modeling with good accuracy and low complexity. It evaluates geometrically the propagation conditions and reflections using the outlines of buildings and foliage, provided by OSM, and the vehicles' ones, provided by SUMO. The propagation parameters used in the considered scenarios are defined according to the recommendations of 3GPP and International Telecommunications Union (ITU). In particular, we select the relative permittivity of ground, buildings, and vehicles based on the ITU measurements in [61]. The PL models for the propagation conditions are defined in Table I. GEMV² outputs the space-time features of the propagation channel, i.e., small and large scale channel components, delays, angles of departure, and angles of arrivals, which are used in (6) to evaluate the SNR for each link pair.

VII. NUMERICAL RESULTS

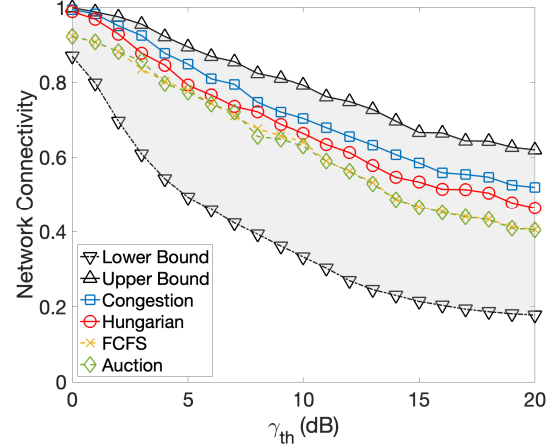
This section shows and discusses the numerical results obtained for the previously presented relaying schemes in terms of network connectivity and computational complexity, which is summarized in Tab. V. The relay selection approaches output the adjacency matrix $\bar{\mathbf{A}}_R$, whose entry $[\bar{\mathbf{A}}_R]_{(i,j)} = 1$ when the direct link between the i th RV and the j th VoI exists or a relay has been successfully allocated, otherwise $[\bar{\mathbf{A}}_R]_{(i,j)} = 0$. The network algebraic connectivity is obtained

Table IV: Vehicles characteristics

Parameter	Range	μ	σ^2
Length	4 – 5 m	4.3 m	0.1 m ²
Width	1.6 – 2 m	1.2 m	0.1 m ²
Height	1.4 – 2 m	1.5 m	0.05 m ²



(a) 100% of vehicles are CAVs

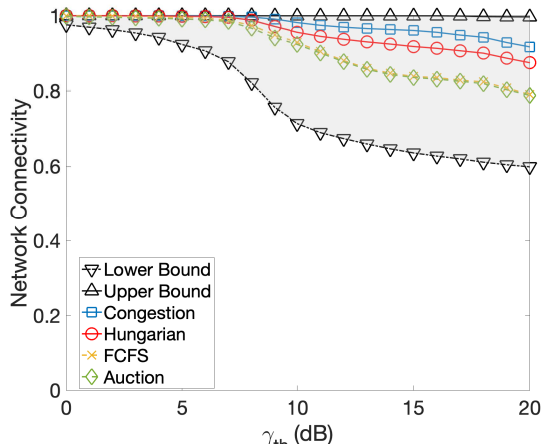


(b) 50% of vehicles are CAVs

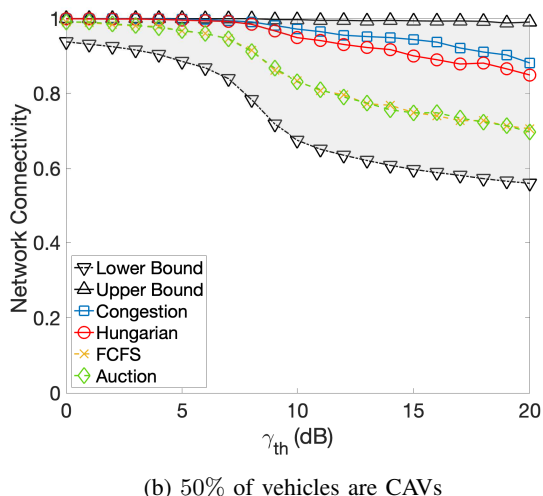
Figure 10: Network connectivity versus SNR γ_{th} for the analyzed relay selection approaches in the intersection scenario when 100% (a) and 50% (b) of vehicles are CAVs.

as in (11) by replacing $\bar{\mathbf{A}}$ with $\bar{\mathbf{A}}_R$. The lower bound of the network connectivity is derived using the average adjacency matrix $\bar{\mathbf{A}}$, while the upper bound is obtained from the second-order average adjacency matrix $\bar{\mathbf{A}}_2$, defined in (13).

The network connectivity for different SNR thresholds γ_{th} and for different relay selection schemes is evaluated for the intersection (Fig. 10) and the roundabout (Fig. 11) scenarios. For all the considered scenarios, it can be noticed that the centralized approaches outperform the distributed ones (Figs. 10-11) at the cost of higher computational complexity, as shown in Fig. 12. Relay selection based on the congestion



(a) 100% of vehicles are CAVs



(b) 50% of vehicles are CAVs

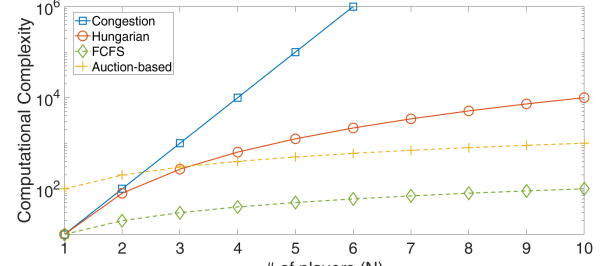
Figure 11: Network connectivity versus SNR γ_{th} for the analysed relay selection approaches in the roundabout scenario when 100% (a) and 50% (b) of vehicles are CAVs.

game shows the best performance attaining the upper bound for a low SNR threshold in the roundabout scenario, which compared to the intersection, exhibits higher connectivity since most of the links are in LoS. Auction-based and FCFS achieve similar network connectivity, while the FCFS schemes show the lowest computational complexity.

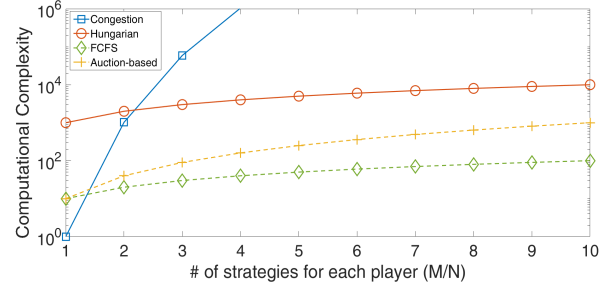
In all the considered scenarios, V2X network has a very large connectivity when all vehicles are CAVs. Vice versa, when the number of nCAVs is comparable to CAVs, we

Table V: Summary of computational complexity

Algorithm	Complexity
Congestion Game	$\mathcal{O}(M^N N^{-N})$
Hungarian Game	$\mathcal{O}(N^2 M)$
FCFS	$\mathcal{O}(M)$
Auction-Based	$\mathcal{O}(T_k M)$



(a)



(b)

Figure 12: Computational complexity of all the algorithms versus number of RV (a) and number of strategies for each RV (b)

observe lower communication reliability due to the frequent blockage. In the coming years, we will experience an increasing market penetration of CAVs in road networks. Results here suggest the strong need to develop robust and resilient relaying techniques; our work provides an innovative framework to evaluate and compare their performances.

VIII. CONCLUSION

Communications at mmW frequencies are expected to support enhanced V2X services. However, link quality degrades easily at high frequencies, also considering that the mobility scenario contributes to repetitive expiration of the LoS condition. To enable beam-type communications it is fundamental to know in advance where to point the beam, by limiting the blockage and by enforcing the LoS condition. Thus, a unified framework for relay selection proves to be a useful tool to overcome blockage drawbacks. In this paper, we propose a novel architecture for relay of opportunity selection in 6G V2X. Here, the high-reliability lower spectrum (FR1) link enables the signalling to exchange the cooperative awareness messages and periodic position information. Based on this collected information and on-board sensors, CAVs estimate the state of nearby objects (nCAVs, buildings, foliage) to predict the dynamic evolution of the LoS. This is exploited to determine the LoS-map, highlighting the most stable links and entering the relay/link selection schemes. Centralized and decentralized opportunistic relay selection approaches' performance is evaluated in terms of network connectivity and numerical complexity. Centralized approaches achieve higher network connectivity, but they are computationally

$$P_{NLoSv} = \iint_{\Omega} \frac{1}{\sqrt{2\pi \det(\tilde{\Sigma}_p)}} \exp\left(-\frac{1}{2} (\mathbf{s}_p - \mathbf{s}_{p,\text{true}})^H \tilde{\Sigma}_p^{-1} (\mathbf{s}_p - \mathbf{s}_{p,\text{true}})\right) d\Omega \quad (22)$$

$$P_{NLoSv} = \left(\mathcal{Q}\left(\frac{x_1 - x_{\text{true}}}{\sigma_x}\right) - \mathcal{Q}\left(\frac{x_2 - x_{\text{true}}}{\sigma_x}\right) \right) \left(\mathcal{Q}\left(\frac{y_1 - y_{\text{true}}}{\sigma_y}\right) - \mathcal{Q}\left(\frac{y_2 - y_{\text{true}}}{\sigma_y}\right) \right) \quad (23)$$

$$f_{\text{SNR}}(\gamma) = \underbrace{P_{LoS} \frac{1}{\sqrt{2\pi\sigma_{sh}^2}} \exp\left(-\frac{(\gamma - A_{LoS}(d))^2}{2(\sigma_{sh}^2)}\right)}_{\text{LoS component } f_{LoS}(\gamma)} + \underbrace{P_{NLoSv} \frac{1}{\sqrt{2\pi(\sigma_v^2 + \sigma_{sh}^2)}} \exp\left(-\frac{(\gamma - (A_{LoS}(d) + A_v))^2}{2(\sigma_v^2 + \sigma_{sh}^2)}\right)}_{\text{NLoSv component } f_{NLoSv}(\gamma)} \quad (24)$$

more demanding than the decentralized ones, which reach a sub-optimal solution with an acceptable complexity. Network connectivity is investigated also considering the impact of nCAVs. The performance results suggest the importance of robust relay selection schemes to counteract blockage. The relay selection schemes proposed here has the capability to guarantee the QoS requirements for the investigated enhanced V2X services. Finally, as future research directions, we will analyze relay selection approaches that account also of the spatial interference and opportunistic time-frequency resource allocation.

APPENDIX A

This section presents the analytical derivation of the SNR distribution. The absence of nCAVs and the assumption of knowing the positions of the VoI and RV, as well as the objects' (e.g., buildings, foliage, and other CAVs) footprint, make the SNR pdf solely dependent on the shadowing component. On the contrary, if nCAVs are part of the considered scenario determining the NLoSv condition (see Remark 2), the SNR pdf also depends on the probability that a single nCAV (or several nCAVs) block(s) the LoS. Therefore, to analytically derive the distribution of the SNR, it is necessary to obtain this probability.

A. Single nCAV Blockage

For sake of simplicity, we first consider the case of a single nCAV, whose state $\tilde{\mathbf{s}}$ at time instant \bar{t} (hereinafter omitted for clarity of notation) is modeled as in Sec. II-B. To derive the blockage probability, we consider only the position information $\tilde{\mathbf{s}}_p = [\tilde{x}, \tilde{y}]$, that is

$$\tilde{\mathbf{s}}_p \sim \mathcal{N}\left(\mathbf{s}_{p,\text{true}}, \tilde{\Sigma}_p\right), \quad (25)$$

where $\tilde{\Sigma}_p$ is defined in (3). The blockage probability P_{NLoSv} is given in (22), where Ω represents the blockage area (see Fig. 4a). The double integral in (22) admits a closed form solution if the blockage area $\Omega \approx [x_1, x_2] \times$

$[y_1, y_2]$ is approximately rectangular and the covariance matrix $\tilde{\Sigma}_p = \text{diag}(\sigma_x^2, \sigma_y^2)$ is diagonal. In this case, the probability of blockage P_{NLoSv} is obtained in (23), where $\mathcal{Q}(\cdot)$ is the Q-function. The LoS probability is obtained by $P_{LoS} = 1 - P_{NLoSv}$. The SNR distribution $f_{\text{SNR}}(\gamma)$ is computed in (24) as a mixture of two normal distributions, which represent the two concurring propagation conditions (LoS and NLoSv). An example of (24) is depicted in Fig. 3. To derive the service probability in (9), we evaluate the cdf of the SNR as

$$F_{\text{SNR}}(\gamma_{\text{th}}) = P_{LoS} F_{LoS}(\gamma_{\text{th}}) + P_{NLoSv} F_{NLoSv}(\gamma_{\text{th}}) \quad (26)$$

where $F_{LoS}(\gamma_{\text{th}})$ and $F_{NLoSv}(\gamma_{\text{th}})$ are the cdfs of LoS and NLoS conditions, respectively. The cdf of a normal distribution $x \sim \mathcal{N}(\mu, \sigma^2)$ can be computed as

$$F_X(x) = 1 - \mathcal{Q}(x) \quad (27)$$

B. Multiple nCAVs Blockage

We generalize the blockage probability derivation to the case of multiple blockers. Assuming the presence of N_b nCAVs, whose state position is defined in (25), the SNR distribution depends on the shadowing component and on the effective number k_b of nCAVs simultaneously blocking the LoS, with $1 \leq k_b \leq N_b$. This can be undertaken as a combinatorial problem. Indeed, to derive the probability $P_{NLoSv}^{(k_b)}$ that k_b out of N_b nCAVs are blocking the LoS, evaluation of all possible combinations is required. The total number of combinations is given by the binomial coefficient

$$N(k_b) = \binom{N_b}{k_b} = \frac{N_b!}{(N_b - k_b)!k_b!}. \quad (28)$$

We refer to the single n th k_b -tuple as \mathbf{b}_n , with $1 \leq n \leq N(k_b)$. The NLoSv probability due to k_b nCAVs effective blockers is

$$P_{NLoSv}^{(k_b)} = \sum_{n=1}^{N(k_b)} \left(\prod_{i \in \mathbf{b}_n} P_{NLoSv}^{(i)} \prod_{j \notin \mathbf{b}_n, j \in [1, N_b]} \left(1 - P_{NLoSv}^{(j)}\right) \right). \quad (29)$$

For example, if we consider $N_b=3$ nCAVs with index $i=\{1, 2, 3\}$, the probability that $k_b = 2$ of them block the LoS according to (29) is

$$P_{NLoSv}^{(2)} = p^{(1)}p^{(2)}(1 - p^{(3)}) + p^{(1)}p^{(3)}(1 - p^{(2)}) + p^{(2)}p^{(3)}(1 - p^{(1)}) \quad (30)$$

where $p^{(i)}$ is the probability that the i th nCAV is blocking the LoS.

Finally, the SNR distribution $f_{SNR}(\gamma)$ is a mixture of Gaussians, computed as

$$f_{SNR}(\gamma) = P_{LoS}f_{LoS}(\gamma) + \sum_{k_b=1}^{N_b} P_{NLoSv}^{(k_b)}f_{NLoSv}^{(k_b)}(\gamma) \quad (31)$$

where $f_{NLoSv}^{(k_b)}(\gamma)$ is the SNR pdf in case of k_b blocking vehicles and $P_{LoS}=1-\sum_{k_b=1}^{N_b} P_{NLoSv}^{(k_b)}$. The mean $A_v^{(k_b)}$ and the variance $\sigma_v^{2(k_b)}$ of the extra attenuation depend on k_b according to the 3GPP recommendations [39]. Similarly, the cdf of the SNR in the multiple nCAVs blockage is obtained as

$$F_{SNR}(\gamma_{th}) = P_{LoS}F_L(\gamma_{th}) + \sum_{k_b=1}^{N_b} P_{NLoSv}^{(k_b)}F_{NLoSv}^{(k_b)}(\gamma_{th}) \quad (32)$$

This result is used to determine the service probability in (9).

ACKNOWLEDGMENT

This research was carried out in the framework of the Huawei-Politecnico di Milano Joint Research Lab. The Authors want to acknowledge the Huawei Milan Research Centre.

REFERENCES

- [1] H. Seo, K. Lee, S. Yasukawa, Y. Peng, and P. Sartori, “Lte evolution for vehicle-to-everything services,” *IEEE Communications Magazine*, vol. 54, no. 6, pp. 22–28, 2016.
- [2] Z. MacHardy, A. Khan, K. Obana, and S. Iwashina, “V2x access technologies: Regulation, research, and remaining challenges,” *IEEE Communications Surveys Tutorials*, vol. 20, no. 3, pp. 1858–1877, 2018.
- [3] J. Wang, J. Liu, and N. Kato, “Networking and communications in autonomous driving: A survey,” *IEEE Communications Surveys Tutorials*, vol. 21, no. 2, pp. 1243–1274, 2019.
- [4] K. Abboud, H. A. Omar, and W. Zhuang, “Interworking of dsrc and cellular network technologies for v2x communications: A survey,” *IEEE Transactions on Vehicular Technology*, vol. 65, no. 12, pp. 9457–9470, 2016.
- [5] R. Molina-Masegosa, J. Gozalvez, and M. Sepulcre, “Configuration of the c-v2x mode 4 sidelink pc5 interface for vehicular communication,” in *2018 14th International Conference on Mobile Ad-Hoc and Sensor Networks (MSN)*, 2018, pp. 43–48.
- [6] 3GPP TS 22.186 v16.2.0, “3rd Generation Partnership Project; technical specification group services and system aspects; study on enhancement of 3GPP support for 5G V2X services (Release 16),” Nov. 2020.
- [7] K. Sakaguchi, R. Fukatsu, T. Yu, E. Fukuda, K. Mahler, R. Heath, T. Fujii, K. Takahashi, A. Khoryae, S. Nagata, and T. Shimizu, “Towards mmwave v2x in 5g and beyond to support automated driving,” 2020.
- [8] 3GPP, “Study on enhancement of 3gpp support for 5g v2x services,” 3rd Generation Partnership Project (3GPP), Tech. Rep. RP22.886, Dec. 2018.
- [9] 3rd Generation Partnership Project. (2021) 3GPP Release 17. [Online]. Available: <https://www.3gpp.org/release-17>
- [10] B. Coll-Perales, M. Gruteser, and J. Gozalvez, “Evaluation of ieee 802.11ad for mmwave v2v communications,” in *2018 IEEE Wireless Communications and Networking Conference Workshops (WCNCW)*, 2018, pp. 290–295.
- [11] A. Molina-Galan, B. Coll-Perales, and J. Gozalvez, “C-v2x assisted mmwave v2v scheduling,” in *2019 IEEE 2nd Connected and Automated Vehicles Symposium (CAVS)*, 2019, pp. 1–5.
- [12] S. Sun, T. S. Rappaport, M. Shafi, P. Tang, J. Zhang, and P. J. Smith, “Propagation models and performance evaluation for 5g millimeter-wave bands,” *IEEE Transactions on Vehicular Technology*, vol. 67, no. 9, pp. 8422–8439, 2018.
- [13] Z. Li, L. Xiang, X. Ge, G. Mao, and H. C. Chao, “Latency and reliability of mmwave multi-hop v2v communications under relay selections,” *IEEE Transactions on Vehicular Technology*, vol. 69, no. 9, pp. 9807–9821, 2020.
- [14] T. S. Rappaport, S. Sun, R. Mayzus, H. Zhao, Y. Azar, K. Wang, G. N. Wong, J. K. Schulz, M. Samimi, and F. Gutierrez, “Millimeter Wave Mobile Communications for 5G Cellular: It Will Work!” *IEEE Access*, vol. 1, pp. 335–349, May 2013.
- [15] A. Awang, K. Husain, N. Kamel, and S. Aïssa, “Routing in vehicular ad-hoc networks: A survey on single- and cross-layer design techniques, and perspectives,” *IEEE Access*, vol. 5, pp. 9497–9517, 2017.
- [16] D. Tian, J. Zhou, Z. Sheng, M. Chen, Q. Ni, and V. C. M. Leung, “Self-organized relay selection for cooperative transmission in vehicular ad-hoc networks,” *IEEE Transactions on Vehicular Technology*, vol. 66, no. 10, pp. 9534–9549, 2017.
- [17] P. Wang, J. Fang, X. Yuan, Z. Chen, and H. Li, “Intelligent reflecting surface-assisted millimeter wave communications: Joint active and passive precoding design,” *IEEE Transactions on Vehicular Technology*, vol. 69, no. 12, pp. 14 960–14 973, 2020.
- [18] B. Gu, Y. Wei, M. Song, F. R. Yu, and Z. Han, “Auction-based relay selection and power allocation in green relay-assisted cellular networks,” *IEEE Transactions on Vehicular Technology*, vol. 68, no. 8, pp. 8000–8011, 2019.
- [19] D. Lin, J. Kang, A. Squicciarini, Y. Wu, S. Gurung, and O. Tonguz, “Mozo: A moving zone based routing protocol using pure v2v communication in vanets,” *IEEE Transactions on Mobile Computing*, vol. 16, no. 5, pp. 1357–1370, 2017.
- [20] X. Wang, T. Jin, L. Hu, and Z. Qian, “Energy-efficient power allocation and q-learning-based relay selection for

relay-aided d2d communication,” *IEEE Transactions on Vehicular Technology*, vol. 69, no. 6, pp. 6452–6462, 2020.

[21] B. Wang, Z. Han, and K. J. R. Liu, “Distributed relay selection and power control for multiuser cooperative communication networks using stackelberg game,” *IEEE Transactions on Mobile Computing*, vol. 8, no. 7, pp. 975–990, 2009.

[22] K. Eshteiwi, G. Kaddoum, K. Ben Fredj, E. Soujani, and F. Gagnon, “Performance analysis of full-duplex vehicle relay-based selection in dense multi-lane highways,” *IEEE Access*, vol. 7, pp. 61 581–61 595, 2019.

[23] H. Guo, B. Makki, D.-T. Phan-Huy, E. Dahlman, M.-S. Alouini, and T. Svensson, “Predictor antenna: A technique to boost the performance of moving relays,” 2021.

[24] J. Wu, H. Lu, Y. Xiang, R. Wu, and F. Wang, “Mbr: A map-based relaying algorithm for reliable data transmission through intersection in vanets,” *IEEE Transactions on Intelligent Transportation Systems*, vol. 20, no. 10, pp. 3661–3674, 2019.

[25] B. Fan, H. Tian, S. Zhu, Y. Chen, and X. Zhu, “Traffic-aware relay vehicle selection in millimeter-wave vehicle-to-vehicle communication,” *IEEE Wireless Communications Letters*, vol. 8, no. 2, pp. 400–403, 2019.

[26] M. Mezzavilla, M. Zhang, M. Polese, R. Ford, S. Dutta, S. Rangan, and M. Zorzi, “End-to-end simulation of 5g mmwave networks,” *IEEE Communications Surveys & Tutorials*, vol. 20, no. 3, pp. 2237–2263, 2018.

[27] G. F. Riley and T. R. Henderson, “The ns-3 network simulator,” in *Modeling and tools for network simulation*. Springer, 2010, pp. 15–34.

[28] N. Patriciello, S. Lagen, B. Bojovic, and L. Giupponi, “An e2e simulator for 5g nr networks,” *Simulation Modelling Practice and Theory*, vol. 96, p. 101933, 2019.

[29] M. Drago, T. Zugno, M. Polese, M. Giordani, and M. Zorzi, “Millicar: An ns-3 module for mmwave nr v2x networks,” in *Proceedings of the 2020 Workshop on ns-3*, 2020, pp. 9–16.

[30] S. Wang, J. Huang, and X. Zhang, “Demystifying millimeter-wave v2x: Towards robust and efficient directional connectivity under high mobility,” in *Proceedings of the 26th Annual International Conference on Mobile Computing and Networking*, 2020, pp. 1–14.

[31] M. Lübke, H. Hamoud, J. Fuchs, A. Dubey, R. Weigel, and F. Lurz, “Channel characterization at 77 ghz for vehicular communication,” in *2020 IEEE Vehicular Networking Conference (VNC)*. IEEE, 2020, pp. 1–4.

[32] G. Thandavarayan, M. Sepulcre, and J. Gozalvez, “Cooperative perception for connected and automated vehicles: Evaluation and impact of congestion control,” *IEEE Access*, vol. 8, pp. 197 665–197 683, 2020.

[33] G. Soatti, M. Nicoli, N. Garcia, B. Denis, R. Raulefs, and H. Wymeersch, “Implicit cooperative positioning in vehicular networks,” *IEEE Transactions on Intelligent Transportation Systems*, vol. 19, no. 12, pp. 3964–3980, 2018.

[34] A. Houenou, P. Bonnifait, V. Cherfaoui, and W. Yao, “Vehicle trajectory prediction based on motion model and maneuver recognition,” in *2013 IEEE/RSJ International Conference on Intelligent Robots and Systems*, 2013, pp. 4363–4369.

[35] G. Xie, H. Gao, L. Qian, B. Huang, K. Li, and J. Wang, “Vehicle trajectory prediction by integrating physics-and maneuver-based approaches using interactive multiple models,” *IEEE Transactions on Industrial Electronics*, vol. 65, no. 7, pp. 5999–6008, 2017.

[36] OpenStreetMap contributors, “Planet dump retrieved from <https://planet.osm.org> ,” <https://www.openstreetmap.org>, 2017.

[37] P. A. Lopez et al., “Microscopic Traffic Simulation using SUMO,” in *IEEE Int. Conf. Intell. Transp. Syst.* IEEE, Dec. 2018. [Online]. Available: <https://elib.dlr.de/124092/>

[38] M. Boban, J. Barros, and O. K. Tonguz, “Geometry-Based Vehicle-to-Vehicle Channel Modeling for Large-Scale Simulation,” *IEEE Trans. Veh. Technol.*, vol. 63, no. 9, pp. 4146–4164, Apr. 2014.

[39] 3GPP TR 37.885 v15.3.0, “Study on evaluation methodology of new Vehicle-to-Everything (V2X) use cases for LTE and NR (Release 15),” Jun. 2019.

[40] J. Choi, V. Va, N. Gonzalez-Prelcic, R. Daniels, C. R. Bhat, and R. W. Heath, “Millimeter-wave vehicular communication to support massive automotive sensing,” *IEEE Commun. Mag.*, vol. 54, no. 12, pp. 160–167, 2016.

[41] ETSI EN 302 637-2 V1.3.2, “Intelligent Transport Systems (ITS); Vehicular Communications; Basic Set of Applications; Part 2: Specification of Cooperative Awareness Basic Service,” Nov. 2014.

[42] M. Shan, K. Narula, Y. F. Wong, S. Worrall, M. Khan, P. Alexander, and E. Nebot, “Demonstrations of cooperative perception: Safety and robustness in connected and automated vehicle operations,” *Sensors*, vol. 21, no. 1, 2021. [Online]. Available: <https://www.mdpi.com/1424-8220/21/1/200>

[43] M. Pfeiffer, G. Paolo, H. Sommer, J. Nieto, R. Siegwart, and C. Cadena, “A data-driven model for interaction-aware pedestrian motion prediction in object cluttered environments,” in *2018 IEEE International Conference on Robotics and Automation (ICRA)*, 2018, pp. 5921–5928.

[44] F. Gustafsson and F. Gunnarsson, “Mobile positioning using wireless networks: possibilities and fundamental limitations based on available wireless network measurements,” *IEEE Signal Processing Magazine*, vol. 22, no. 4, pp. 41–53, 2005.

[45] ITU-R, “Propagation by diffraction, = International Telecommunication Union Radio Sector(ITU-R), year=2019,” Tech. Rep. P.526, Ago.

[46] J. Goldhirsh and W. J. Vogel, “Handbook of propagation effects for vehicular and personal mobile satellite systems,” *NASA Reference Publication*, vol. 1274, pp. 40–67, 1998.

[47] M. Mizmizi, F. Linsalata, M. Brambilla, F. Morandi, K. Dong, M. Magarini, M. Nicoli, M. N. Khormuji, P. Wang, R. A. Pitaval, and U. Spagnolini, “Fastening the initial access in 5g nr sidelink for 6g v2x networks,”

Vehicular Communications, p. 100402, 2021. [Online]. Available: <https://www.sciencedirect.com/science/article/pii/S2214209621000711>

[48] S. Lien, D. Deng, C. Lin, H. Tsai, T. Chen, C. Guo, and S. Cheng, “3gpp nr sidelink transmissions toward 5g v2x,” *IEEE Access*, vol. 8, pp. 35 368–35 382, 2020.

[49] M. T. Rahman, T. Karamat, S. Givigi, and A. Noureldin, “Improving multisensor positioning of land vehicles with integrated visual odometry for next-generation self-driving cars,” *Journal of Advanced Transportation*, vol. 2018, 2018.

[50] J. Ji, A. Khajepour, W. W. Melek, and Y. Huang, “Path planning and tracking for vehicle collision avoidance based on model predictive control with multiconstraints,” *IEEE Transactions on Vehicular Technology*, vol. 66, no. 2, pp. 952–964, 2017.

[51] A. Jamakovic and S. Uhlig, “On the relationship between the algebraic connectivity and graph’s robustness to node and link failures,” in *2007 Next Generation Internet Networks*. IEEE, 2007, pp. 96–102.

[52] Y. Hao, S. Pan, Y. Qiao, and D. Cheng, “Cooperative control via congestion game approach,” *IEEE Transactions on Automatic Control*, vol. 63, no. 12, pp. 4361–4366, 2018.

[53] C. A. Meyers and A. S. Schulz, “The complexity of congestion games,” *Massachusetts Institute of Technology, Cambridge*, pp. 1–16, 2008.

[54] R. E. Burkard and E. Cela, “Linear assignment problems and extensions,” in *Handbook of combinatorial optimization*. Springer, 1999, pp. 75–149.

[55] J. Wang, P. He, and W. Coo, “Study on the hungarian algorithm for the maximum likelihood data association problem,” *Journal of Systems Engineering and Electronics*, vol. 18, no. 1, pp. 27–32, 2007.

[56] W. Zhong, K. Xie, Y. Liu, C. Yang, and S. Xie, “Multi-resource allocation of shared energy storage: A distributed combinatorial auction approach,” *IEEE Transactions on Smart Grid*, vol. 11, no. 5, pp. 4105–4115, 2020.

[57] M. M. Zavlanos, L. Spesivtsev, and G. J. Pappas, “A distributed auction algorithm for the assignment problem,” in *2008 47th IEEE Conference on Decision and Control*, 2008, pp. 1212–1217.

[58] T. S. Rappaport, F. Gutierrez, E. Ben-Dor, J. N. Murdock, Y. Qiao, and J. I. Tamir, “Broadband millimeter-wave propagation measurements and models using adaptive-beam antennas for outdoor urban cellular communications,” *IEEE Transactions on Antennas and Propagation*, vol. 61, no. 4, pp. 1850–1859, 2013.

[59] M. R. Akdeniz, Y. Liu, M. K. Samimi, S. Sun, S. Rangan, T. S. Rappaport, and E. Erkip, “Millimeter wave channel modeling and cellular capacity evaluation,” *IEEE Journal on Selected Areas in Communications*, vol. 32, no. 6, pp. 1164–1179, 2014.

[60] 3GPP, “User equipment (ue) radio transmission and reception; part 2: Range 2 standalone,” 3rd Generation Partnership Project (3GPP), Tech. Rep. TS 38.101, Oct. 2020.

[61] ITU, “Effects of building materials and structures on radiowave propagation above about 100 mhz,” International Telecommunication Union (ITU), Tech. Rep. ITU-R P.2040-1, May 2015.